Split Archimedean spiral metasurface for controllable GHz asymmetric transmission

Song, Qing Hua; Wu, Pin Chieh; Zhu, Wei Ming; Zhang, Wu; Shen, Ze Xiang; Chong, Peter Han Joo; Liang, Qing Xuan; Tsai, D. P.; Bourouina, Tarik; Leprince-Wang, Yamin; Liu, Ai Qun

2019

https://hdl.handle.net/10356/85227

https://doi.org/10.1063/1.5084329

Applied Physics Letters

Split Archimedean spiral metasurface for controllable GHz asymmetric transmission

Q. H. Song, P. C. Wu, W. M. Zhu, W. Zhang, Z. X. Shen, P. H. J. Chong (iD), Q. X. Liang, D. P. Tsai, T. Bourouina, Y. Leprince-Wang (iD), and A. Q. Liu

View Online   Export Citation   CrossMark

ARTICLES YOU MAY BE INTERESTED IN

Split Archimedean spiral metasurface for controllable GHz asymmetric transmission

Q. H. Song,[1,2] P. C. Wu,[2] W. M. Zhu,[3,a)] W. Zhang,[2] Z. X. Shen,[2] P. H. J. Chong,[4] (iD) Q. X. Liang,[5] D. P. Tsai,[6] T. Bourouina,[7] Y. Leprince-Wang,[1,a)] (iD) and A. Q. Liu[2,a)]

AFFILIATIONS

[1]Université Paris-Est, ESYCOM, UPEM, F-77454 Marne-la-Vallée, France
[2]School of Electrical and Electronic Engineering, Nanyang Technological University, Singapore 639798
[3]School of Optoelectronic Information, University of Electronic Science and Technology of China (UESTC), Chengdu 610054, China
[4]Department of Electrical and Electronic Engineering, Auckland University of Technology, Auckland 1010, New Zealand
[5]School of Mechanical Engineering, Xi'an Jiaotong University, Xi'an 710049, China
[6]Research Center for Applied Sciences, Academia Sinica, Taipei 11529, Taiwan
[7]Université Paris-Est, ESYCOM, ESIEE, F-93162 Noisy-le-Grand, France

[a)]Electronic addresses: zhuweiming@uestc.edu.cn; Yamin.Leprince@u-pem.fr; and eaqliu@ntu.edu.sg.

ABSTRACT

A chiral metasurface, which obtains chirality through a subwavelength artificial structure, is essential for realizing asymmetric transmission in the application of enantioselective sensing, spin-dependent light emission, and other polarization control systems. Here, we studied a split Archimedean spiral metasurface, which can control the propagating wave from asymmetric transmission to symmetric transmission for linear polarized light. As a proof of concept, a dual-band asymmetric transmission is demonstrated in the GHz region using the coupling of the split spiral structures. The maximum asymmetric transmission parameter reaches 53%. By manipulating the height of the split spiral structures using microfluidic technology, a broadband asymmetric transmission is obtained with the bandwidth of 25.9%. Meanwhile, the asymmetric transmission can be controlled from 50% to 0%, enabling the propagation wave from asymmetric transmission to symmetric transmission. Furthermore, the asymmetric transmission is maintained when the metasurface is bent into different curvatures, promising high potential applications for optical isolation, one-way glass, and optical interconnects.

Published under license by AIP Publishing. https://doi.org/10.1063/1.5084329

A chiral material exhibits asymmetric transmission which allows the electromagnetic wave of cross-polarization to transmit in one direction, while blocking the transmission of the same polarization in the opposite direction.[1] Possible applications include microwave and optical isolation, optical interconnects, ultrafast information processing, and integrated photonic circuits. The research of asymmetric transmission for circularly polarized light has been reported in planar chiral metasurfaces.[2–4] However, such planar chiral metasurfaces only exhibit chirality in two-dimensional space instead of three-dimensional (3D), in which the asymmetric transmission only works for circular polarized light instead of linear polarized light.[5] Generally speaking, the chirality in three-dimensional can be introduced by applying the supporting substrate underneath the metasurface structures.[6] However, this effect of symmetry breaking is negligible for observable asymmetric transmission. In order to unambiguously

enhance the effect of asymmetric transmission, it is suggested to break the symmetry in the propagation direction of the metamolecule itself rather than relying on the effect of the supporting substrate.[5,7–11] However, the rigid substrate based chiral metasurface suffers from limited tunability and the transition from asymmetric transmission to symmetric transmission is also lagging behind.

Metasurfaces are usually composed of solid metallic structures or high permittivity dielectrics on solid substrates, whose tunability is highly constrained by the material rigidity, tuning the free carrier density,[12–15] thermal effect,[16–19] optical pump,[20–23] using micromachined technology,[24–27] etc.[28–34] Soft materials based on polydimethylsiloxane (PDMS) are further introduced to control the metasurface with more flexibility.[35,36] However, they are usually controlled by stretching the substrate, which inevitably suffers the inhomogeneous stretching force on each metamolecule and the unfixed size of the metasurface. By

incorporating with microfluidic technology, one can create control channels into the PDMS substrate, leading to individual control of each metamolecule.[37–40] Moreover, a water-resonator-based metasurface is proposed, whose metamolecules can be controlled in 3D.[41] However, water is quite absorptive, which is not suitable for transmitted applications. Here, we introduce a split Archimedean spiral metasurface (SASM) for controlling asymmetric transmission by constructing an array of spiral structures patterned on both sides of PDMS. Compared to the previous work using a rigid substrate,[42] the SASM is designed to be controlled by using microfluidic technology in real time. The microfluidic system reconfigures the height of spiral structures, which offers a promising way for dynamic manipulation on asymmetric transmission at will. Furthermore, the split Archimedean spiral metasurface can be deformed in the arbitrary curvature to cover on various shaped structures due to the flexibility of PDMS. The mirror image of the split spiral structures is not congruent with itself, leading to a chiral characteristic. By reconfiguring the spiral structures, the chirality of the metasurface can be manipulated, resulting in a controllable asymmetric transmission.
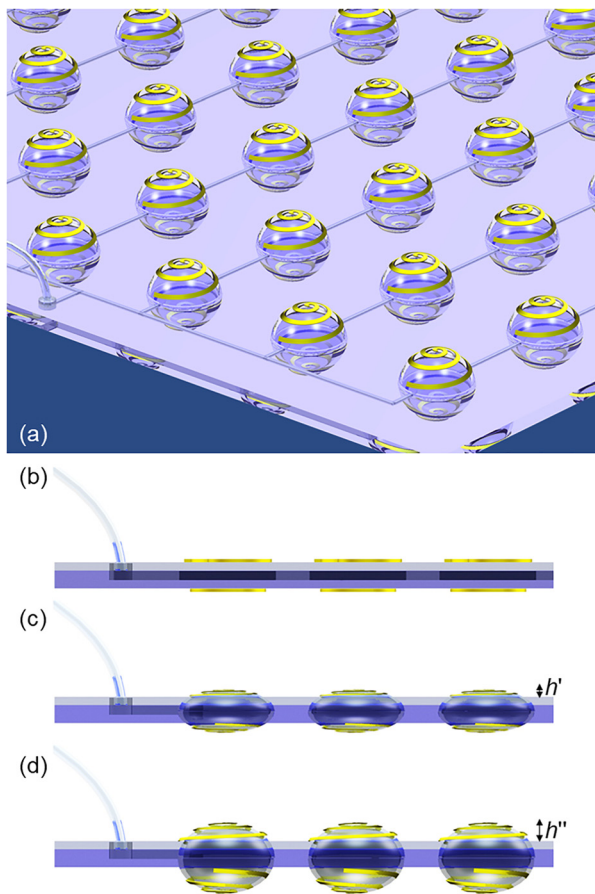

FIG. 1. Schematic of the SASM. (a) Perspective view of the SASM. (b) Side view of the metasurface without air injection. (c) The SAS structures can be deformed to 3D by applying air pressure into the microfluidic channel. (d) The height of SAS structures could be actively controlled by applying different air pressures.

The split Archimedean spiral metasurface incorporating with microfluidic technology is illustrated in Fig. 1(a), and the dimension of each single metamolecule is shown in Fig. S1 in the supplementary material. The metamolecule consists of an air reservoir formed by bonding two PDMS layers together and two Archimedean spiral metallic structures deposited on both sides of PDMS, which is called the split Archimedean spiral (SAS) structure. The original state of the split Archimedean spiral metasurface is planar as shown in Fig. 1(b) without air injection. The SASM is chiral and exhibits asymmetric transmission. Since there is an air reservoir between the two spiral structures, when the air is injected into the reservoir, the PDMS membrane is expanded and formed a PDMS sphere cap due to the air pressure. The expanded PDMS membrane stretches the SAS structures out of plane, leading to a 3D spiral structure. The heights of both PDMS membranes under top and bottom spiral structures are the same so that when the air is injected into the microfluidic channel, both spiral structures will be deformed with an equal height of h. By applying different air pressures, the PDMS membrane can be expanded or contracted, resulting in a reversible process to flexibly reconfigure the height of the spiral structure h as shown in Figs. 1(c) and 1(d). Thereby, the chirality of the SASM can be dynamically controlled, which enables the manipulation of the asymmetric transmission.

The optical response of the SASM is simulated by CST microwave studio with the periodic boundary condition. The SAS structures are patterned on both sides of the low permittivity dielectric material, PDMS, forming a metal/PDMS/metal sandwich structure. The relative permittivity of PDMS is 2.83, and the conductivity of gold is 4.561×10^7 s/m. Simulation results of the forward and backward transmission of cross-polarization when the height of the SAS structures is changed from $h = 0$ mm to $h = 1$ mm are shown in Fig. 2. Since the SASM is chiral, the forward and backward transmission is different, i.e., $T_{yx}^f \neq T_{yx}^b$ (the superscripts f and b indicate the microwave incidence in the forward and backward propagation directions, respectively). When the SAS structures are planar ($h = 0$ mm), two resonance peaks, induced by the coupling between the two spiral structures, occur in the forward transmission spectrum at $f_1 = 28$ GHz and $f_2 = 37.2$ GHz, respectively, as shown in the red curve of Fig. 2(a). The coupling between these two spirals contributes to the resonances at certain frequencies for the metasurface, which refers to plasmonic hybridization.[43] A bonding mode in the SAS structures is induced at the lower frequency f_1 as shown in Figs. 2(c) and 2(d), while an antibonding mode is induced at the higher frequency f_2 as shown in Figs. 2(e) and 2(f). The strength of the current under forward incidence as shown in Figs. 2(c) and 2(e) is much stronger than that under backward incidence as shown in Figs. 2(d) and 2(f), resulting in higher forward transmission than backward transmission as shown in Figs. 2(a) and 2(b). The height of the SAS structures can be controlled by applying different air pressures in the microfluidic channels, leading to a 3D chiral structure. The distance between the two spiral structures will be enlarged when the air pressure is increased so that the coupling of the two resonant frequencies will be decreased as shown in Fig. 2(a). f_1 will blue shift to 30.5 GHz and f_2 will red shift to 35.5 GHz when $h = 1$ mm. The strength of the current under forward incidence is still larger than that under backward incidence as shown in Fig. S2 in the supplementary material. Figure S3 shows the asymmetric transmission parameter ($\Delta_{lin}^{(x)} = |T_{yx}^f|^2 - |T_{yx}^b|^2$) when the height of the SAS structures is
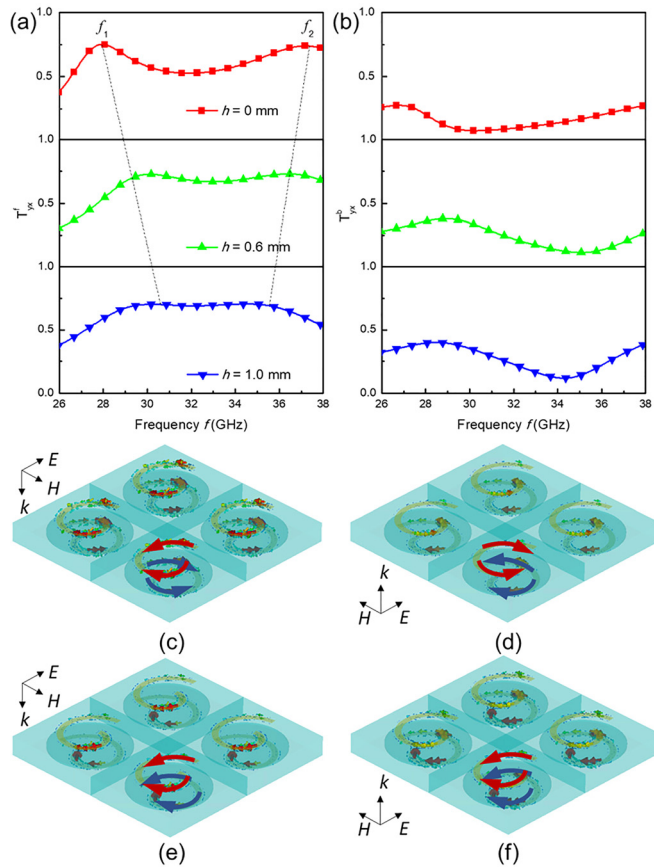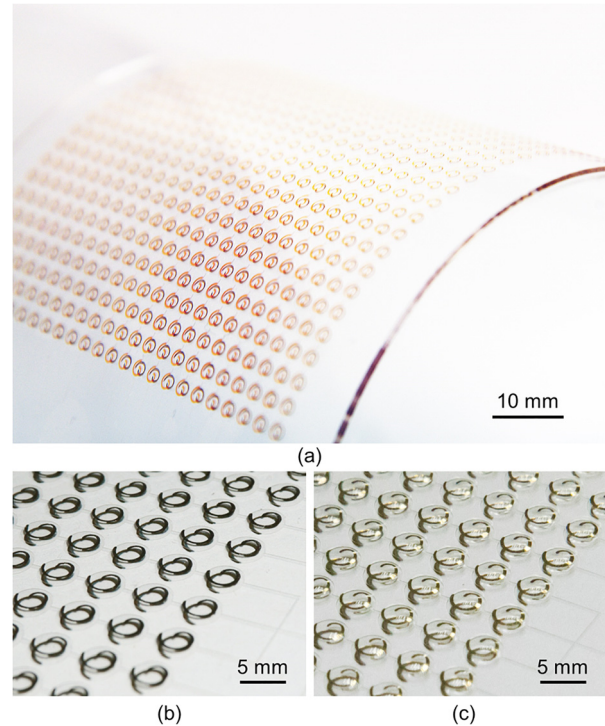
FIG. 2. Simulation results of the SASM. (a) Forward transmission spectra T^f_{yx} and (b) backward transmission spectra T^b_{yx} when the height of the SAS structures is changed from $h = 0$ mm to $h = 1.0$ mm. Current distribution when $h = 0$ mm with (c) forward transmission at f_1, (d) backward transmission at f_1, (e) forward transmission at f_2, and (f) backward transmission at f_2. The red arrow indicates the current of the top spiral structures, and the blue arrow indicates the current of the bottom spiral structures.

FIG. 3. Fabrication results of the SASM. (a) SASM with the arbitrary curvature. The height of the SAS structures is changed continuously from (b) $h = 0$ mm to (c) $h = 1.4$ mm by applying air pressure.

changed from $h = 0$ mm to $h = 1.4$ mm. It can be observed that $\Delta^{(x)}_{lin}$ is dual-band when $h = 0$ and the maximum $\Delta^{(x)}_{lin}$ reaches over 52.1%. When the height of the SAS structures increases, these two bands will merge with each other and become a broadband asymmetric transmission. The bandwidth reaches 23.6% with $\Delta^{(x)}_{lin}$ higher than 40%. At the frequency of 37 GHz, the asymmetric transmission exhibits large tunability, which can be tuned from 50% to 0% when the height of the SAS structures is changed from 0 mm to 1.4 mm as shown in Fig. S3(b) in the supplementary material. In this way, the propagation wave of the SASM can be controlled from asymmetric transmission to symmetric transmission.

The fabrication processes and results of the SASM are shown in Fig. S4 in the supplementary material and Fig. 3, respectively. The metal structure uses gold, which is anchored on a PDMS membrane with air reservoirs connected by microchannels. The width of the air channels is 0.8 mm, and the diameter of the air reservoir is 4 mm. The whole sample of SASM consists of 24×24 elements with a 5-mm periodic, and the total footprint of the SASM is 120 mm $\times$ 120 mm.

The original state of the SAS structures is planar as shown in Fig. 3(b). When the air pressure is applied in the microfluidic channels, the PDMS membrane is expanded, leading to a controllable height of the SAS structures as shown in Fig. 3(c). The SASM can also be bent into arbitrary curved surfaces due to the flexibility of the PDMS. The measurement of the SASM is carried out in the anechoic chamber room. The transmission measurement setup is shown in Fig. S5(a) in the supplementary material. The experimental results of the SASM are shown in Fig. 4. A dual-band transmission spectrum is observed with forward incidence as shown in Fig. 4(a). When the height of the SAS structures is increased, the distance between these two bands will be decreased. The backward transmission is relatively low as shown in Fig. 4(b). The maximum $\Delta^{(x)}_{lin}$ is around 50% as shown in Fig. 4(c). It is shown that the measured bandwidth of the asymmetric transmission is 25.9% with $\Delta^{(x)}_{lin}$ higher than 40% when $h = 0.6$ mm. At the frequency of 37 GHz, a large tunability of asymmetric transmission is realized as shown in Fig. 4(d), which agrees well with the simulated results. The asymmetric transmission can be tuned from 50% to 0% when the height of the SAS structures is changed from 0 to 1.4 mm. The slight mismatch between the simulated and measured results is induced by fabrication error. The spiral structures are not uniform due to inhomogeneous pressures in the air reservoirs.

Here, we also investigate the asymmetric transmission of SASM under oblique incidence. The experimental setup for the oblique incident measurement is shown in Fig. S5(b) in the supplementary material. The transmission with different incident angles can be measured by tilting the sample with an angle of θ. The incident microwave is the
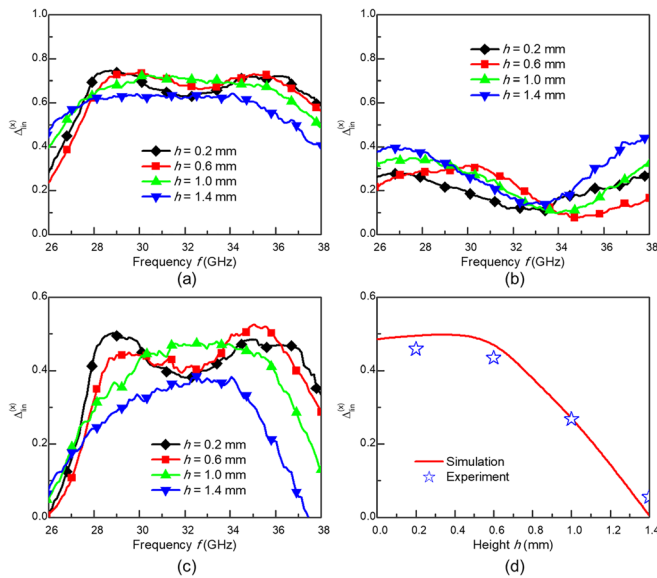
FIG. 4. Experimental results of the SASM when the height of the SAS structures is changed from 0 to 1.4 mm. (a) Forward transmission. (b) Backward transmission. (c) $\Delta_{lin}^{(x)}$. (d) $\Delta_{lin}^{(x)}$ as a function of h at the frequency of 37 GHz.

TE mode. The backward transmission can be measured by flipping over the sample. The experimental results of the forward and backward transmission when the incident angle is changed from 0^0 to 45^0 with the height of the SAS structures $h = 1.0$ mm are shown in Figs. S6(a) and S6(b) in the supplementary material, respectively. The forward transmission is much higher than the backward transmission. When the incident angle increases, the bandwidth of the forward transmission becomes narrow. The backward transmission remains at a low level when the incident angle is increasing.

The asymmetric transmission is also demonstrated with different curvatures of the SASM. Since the PDMS is soft, the SASM can be bent into different curvatures. The experimental setup for the curved SASM is shown in Fig. S5(c) in the supplementary material. The extent of bending is defined as the overall height of the sample d. Likewise, the backward transmission is measured by flipping over the sample. The height of the SAS structures is $h = 1.0$ mm. The experimental results of the forward and backward transmission when h is changed from 10 mm to 40 mm are shown in Figs. S7(a) and S7(b) in the supplementary material, respectively. $\Delta_{lin}^{(x)}$ is shown in Fig. S7(c) in the supplementary material. When d is increasing, $\Delta_{lin}^{(x)}$ remains at a high level in a broad bandwidth.

In conclusion, a SASM for controllable asymmetric transmission is demonstrated experimentally. Two layers of spiral structures are deposited on both sides of the PDMS, whose height can be controlled by injecting different air pressures in the PDMS microchannel, so that the asymmetric transmission can be manipulated. The maximum $\Delta_{lin}^{(x)}$ of the proposed SASM reaches 53%. The measured bandwidth of the asymmetric transmission is 25.9% with $\Delta_{lin}^{(x)}$ higher than 40%. A large tunability of the asymmetric transmission is realized from 50% to 0%, when the height of the SAS structures is controlled from 0 mm to 1.4 mm. The high asymmetric transmission is preserved with oblique incidence from $0°$ to $45°$. In addition, the asymmetric transmission remains at a high level under different curvatures of the curved SASM. Such SASM has potential applications for optical isolation, one-way glass, and is highly valuable for the development of nanophotonic devices.

See the supplementary material for the supporting content.

REFERENCES

[1]Z. Li, M. Mutlu, and E. Ozbay, J. Opt. **15**, 023001 (2013).

[2]A. S. Schwanecke, V. A. Fedotov, V. V. Khardikov, S. L. Prosvirnin, Y. Chen, and N. I. Zheludev, Nano Lett. **8**, 2940 (2008).

[3]V. A. Fedotov, A. S. Schwanecke, N. I. Zheludev, V. V. Khardikov, and S. L. Prosvirnin, Nano Lett. **7**, 1996 (2007).

[4]S. A. Dyakov, V. A. Semenenko, N. A. Gippius, and S. G. Tikhodeev, Phys. Rev. B **98**, 235416 (2008).

[5]C. Menzel, C. Helgert, C. Rockstuhl, E.-B. Kley, A. Tünnermann, T. Pertsch, and F. Lederer, Phys. Rev. Lett. **104**, 253902 (2010).

[6]S. I. Maslovski, D. K. Morits, and S. A. Tretyakov, J. Opt., A **11**, 074004 (2009).

[7]M. Kang, J. Chen, H.-X. Cui, Y. Li, and H.-T. Wang, Opt. Express **19**, 8347 (2011).

[8]M. Mutlu, A. E. Akosman, A. E. Serebryannikov, and E. Ozbay, Opt. Express **19**, 14290 (2011).

[9]F. Dincer, C. Sabah, M. Karaaslan, E. Unal, M. Bakir, and U. Erdiven, Prog. Electromagn. Res. **140**, 227 (2013).

[10]J. Shi, X. Liu, S. Yu, T. Lv, Z. Zhu, H. Feng Ma, and T. Jun Cui, Appl. Phys. Lett. **102**, 191905 (2013).

[11]M. Mutlu, A. E. Akosman, A. E. Serebryannikov, and E. Ozbay, Phys. Rev. Lett. **108**, 213905 (2012).

[12]Y. C. Jun, E. Gonzales, J. L. Reno, E. A. Shaner, A. Gabbay, and I. Brener, Opt. Express **20**, 1903 (2012).

[13]K. Fan, H. Y. Hwang, M. Liu, A. C. Strikwerda, A. Sternbach, J. Zhang, X. Zhao, X. Zhang, K. A. Nelson, and R. D. Averitt, Phys. Rev. Lett. **110**, 217404 (2013).

[14]T. Lewi, P. P. Iyer, N. A. Butakov, A. A. Mikhailovsky, and J. A. Schuller, Nano Lett. **15**, 8188 (2015).

[15]H.-T. Chen, W. J. Padilla, M. J. Cich, A. K. Azad, R. D. Averitt, and A. J. Taylor, Nat. Photonics **3**, 148 (2009).

[16]H. Tao, A. C. Strikwerda, K. Fan, W. J. Padilla, X. Zhang, and R. D. Averitt, Phys. Rev. Lett. **103**, 147401 (2009).

[17]R. Singh, A. K. Azad, Q. X. Jia, A. J. Taylor, and H.-T. Chen, Opt. Lett. **36**, 1230 (2011).

[18]J. Zhu, J. Han, Z. Tian, J. Gu, Z. Chen, and W. Zhang, Opt. Commun. **284**, 3129 (2011).

[19]T. Han, X. Bai, J. T. L. Thong, B. Li, and C.-W. Qiu, Adv. Mater. **26**, 1731 (2014).

[20]H.-T. Chen, J. F. O'hara, A. K. Azad, A. J. Taylor, R. D. Averitt, D. B. Shrekenhamer, and W. J. Padilla, Nat. Photonics **2**, 295 (2008).

[21]N.-H. Shen, M. Massaouti, M. Gokkavas, J.-M. Manceau, E. Ozbay, M. Kafesaki, T. Koschny, S. Tzortzakis, and C. M. Soukoulis, Phys. Rev. Lett. **106**, 037403 (2011).

[22]Y. F. Yu, A. Y. Zhu, R. Paniagua-Domínguez, Y. H. Fu, B. Luk'yanchuk, and A. I. Kuznetsov, Laser Photonics Rev. **9**, 412 (2015).

[23]K. Dholakia, P. Reece, and M. Gu, Chem. Soc. Rev. **37**, 42 (2008).

[24]A. Q. Liu, W. M. Zhu, D. P. Tsai, and N. I. Zheludev, J. Opt. **14**, 114009 (2012).

[25]W. M. Zhu, A. Q. Liu, T. Bourouina, D. P. Tsai, J. H. Teng, X. H. Zhang, G. Q. Lo, D. L. Kwong, and N. I. Zheludev, Nat. Commun. **3**, 1274 (2012).

[26]X. Liu and W. J. Padilla, Adv. Opt. Mater. **1**, 559 (2013).

[27]W. Zhang, W. M. Zhu, H. Cai, M.-L. J. Tsai, G.-Q. Lo, D. P. Tsai, H. Tanoto, J. H. Teng, X.-H. Zhang, D.-L. Kwong, and A. Q. Liu, IEEE J. Sel. Top. Quantum **19**, 4700306 (2013).

[28]K. Chen, Y. Feng, F. Monticone, J. Zhao, B. Zhu, T. Jiang, L. Zhang, Y. Kim, X. Ding, S. Zhang, A. Alù, and C.-W. Qiu, Adv. Mater. **29**, 1606422 (2017).

[29]L. Li, T. Jun Cui, W. Ji, S. Liu, J. Ding, X. Wan, Y. B. Li, M. Jiang, C.-W. Qiu, and S. Zhang, Nat. Commun. **8**, 197 (2017).

[30]L. Yan, W. Zhu, M. F. Karim, H. Cai, A. Y. Gu, Z. Shen, P. H. J. Chong, D.-L. Kwong, C.-W. Qiu, and A. Q. Liu, Adv. Mater. **30**, 1802721 (2018).

[31]Y. Z. Shi, S. Xiong, Y. Zhang, L. K. Chin, Y. Y. Chen, J. B. Zhang, T. H. Zhang, W. Ser, A. Larson, L. S. Hoi, J. H. Wu, T. N. Chen, Z. C. Yang, Y. L. Hao, B. Liedberg, P. H. Yap, D. P. Tsai, C. W. Qiu, and A. Q. Liu, Nat. Commun. **9**, 815 (2018).

[32]Y. Z. Shi, S. Xiong, L. K. Chin, J. B. Zhang, W. Ser, J. H. Wu, T. N. Chen, Z. C. Yang, Y. L. Hao, B. Liedberg, P. H. Yap, D. P. Tsai, C. W. Qiu, and A. Q. Liu, Sci. Adv. **4**, eaao0773 (2018).

[33]Q. Song, Z. Shen, and J. Lu, IEEE Trans. Antennas Propag. **66**, 4687 (2018).

[34]H. T. Zhao, Y. Zhang, P. Y. Liu, P. H. Yap, W. Ser, and A. Q. Liu, Sens. Actuator, B **280**, 16 (2019).

[35]P. Gutruf, C. Zou, W. Withayachumnankul, M. Bhaskaran, S. Sriram, and C. Fumeaux, ACS Nano **10**, 133 (2016).

[36]S. Aksu, M. Huang, A. Artar, A. A. Yanik, S. Selvarasah, M. R. Dokmeci, and H. Altug, Adv. Mater. **23**, 4422 (2011).

[37]W. Zhu, Q. Song, L. Yan, W. Zhang, P.-C. Wu, L. K. Chin, H. Cai, D. P. Tsai, Z. X. Shen, T. W. Deng, S. K. Ting, Y. Gu, G. Q. Lo, D. L. Kwong, Z. C. Yang, R. Huang, A.-Q. Liu, and N. Zheludev, Adv. Mater. **27**, 4739 (2015).

[38]W. Zhang, Q. Song, W. Zhu, Z. Shen, P. Chong, D. P. Tsai, C. Qiu, and A. Q. Liu, Adv. Phys. X **3**, 1417055 (2018).

[39]Q. H. Song, W. M. Zhu, P. C. Wu, W. Zhang, Q. Y. S. Wu, J. H. Teng, Z. X. Shen, P. H. J. Chong, Q. X. Liang, Z. C. Yang, D. P. Tsai, T. Bourouina, Y. Leprince-Wang, and A. Q. Liu, APL Mater. **5**, 066103 (2017).

[40]P. C. Wu, W. Zhu, Z. X. Shen, P. H. J. Chong, W. Ser, D. P. Tsai, and A.-Q. Liu, Adv. Opt. Mater. **5**, 1600938 (2017).

[41]Q. Song, W. Zhang, P. C. Wu, W. Zhu, Z. X. Shen, P. H. J. Chong, Q. X. Liang, Z. C. Yang, Y. L. Hao, H. Cai, H. F. Zhou, Y. Gu, G. Q. Lo, D. P. Tsai, T. Bourouina, Y. Leprince-Wang, and A. Q. Liu, Adv. Opt. Mater. **5**, 1601103 (2017).

[42]L. Xie, H.-L. Yang, X. Huang, and Z. Li, Prog. Electromagn. Res. **141**, 645 (2013).

[43]E. Prodan, C. Radloff, N. J. Halas, and P. Nordlander, Science **302**, 419–422 (2003).